Available online at www.sciencedirect.com
SCIENCE DIRECT®
International Journal of Solids and Structures 41 (2004) 6725–6744
INTERNATIONAL JOURNAL OF SOLIDS and STRUCTURES
www.elsevier.com/locate/ijsolstr

Dynamic interaction between multiple cracks and a circular hole swept by SH waves

Jian-Fei Lu [a,b,*], Andrzej Hanyga [b]

[a] Mathematics and Physics College of Jiangsu University, Zhenjiang, Jiangsu 212013, PR China
[b] Institute of Earth Science, University of Bergen, Allegaten 41, Bergen N5007, Norway

Received 13 May 2004
Available online 10 July 2004

Abstract

The focus of this contribution is to develop a hypersingular integral equation method (HIEM) to solve the dynamic interaction between multiple cracks and a circular hole illuminated by plane SH waves. The cracks can be in arbitrary positions; in particular, they can terminate at the boundary of the circular hole. In order to solve the proposed problem, the Green's function of a point harmonic force applied at an infinite plane with a circular hole is obtained by the Graf formula and the wave function expansion method. In order to construct the hypersingular integral equations for the cracks, the Green's function is separated into a closed form singular part and a regular part. On the basis of the reciprocity principle as well as the obtained Green's function, the hypersingular integral equations for the cracks are obtained. Numerical solution of the hypersingular integral equations yields the dynamic stress intensity factors (DSIF) at the crack tips. Comparison of present results with known results verifies the proposed method. Some numerical examples are presented in the paper.

Keywords: Crack; Circular hole; SH wave; Hypersingular integral equations; Green's function; Dynamic stress intensity factor (DSIF)

1. Introduction

Stress concentration around holes is an important problem for civil engineering, earthquake engineering and mechanical engineering and has, therefore, been investigated by numerous researchers using various methods. There are large amount of investigations concerning hole problems, the most important contributions of which were summarized in the two well-known works (Savin, 1961; Muskhelishvili, 1953b). In the middle of 1950s, due to the requirements of practical engineering, the dynamic stress concentration around holes began to attract the attention of many researchers (Pao and Mow, 1973). For example, the dynamic response of a circular tunnel was investigated by Lee and Trifunac (1979) using the wave function

* Corresponding author. Address: Mathematics and Physics College of Jiangsu University, Zhenjiang, Jiangsu 212013, PR China. Tel.: +47-55583424; fax: +47-55583660.
E-mail addresses: ljfdoctor@yahoo.com, jianfei.lu@geo.uib.no (J.-F. Lu).

0020-7683/$ - see front matter © 2004 Elsevier Ltd. All rights reserved.
doi:10.1016/j.ijsolstr.2004.05.033

expansion method; the stress concentration around multiple circular holes is studied by Providakis et al. (1993) by using boundary element method (BEM) and Laplace transform method. For both the static and the dynamic hole problems, the major concern is to calculate stress concentration factors along hole boundaries, which are of great importance for engineering designs. Physically, the stress concentration around hole boundaries may generate cracks near boundaries. As a result, the interaction between holes and cracks has been a very popular topic for many researchers for a long time. For example, by using complex method and superposition method, a general solution is obtained to the problem of the interaction between a main crack and an arbitrarily located and oriented elliptical hole near its tip under mode III loading conditions (Gong and Meguid, 1991). The boundary integral equation (BEM) method was formulated to evaluate the stress intensity factors of a crack approaching a curvilinear hole in an anisotropic plane under arbitrary loadings (Liaw and Kamel, 1991). By using complex variables method and Fredholm integral equation method, the interaction between multiple cracks and a circular hole under antiplane deformation was studied by Chen and Wang (1986). Owing to the inherent difficulties involved in the dynamic crack–hole interaction, the researches about crack–hole interaction have been mainly limited to the static case so far. However, from the practical point of view, the dynamic crack–hole interaction problems are crucial for the earthquake engineering and nondestructive evaluation (NDE).

To date, there are many investigations concerning the interaction between cracks and elastic waves. For instance, the scattering of elastic wave by a single crack and multiple cracks were investigated by Loeber and Sih (1968), Gross and Zhang (1988), respectively. The dynamic response of an interface crack has been addressed by Qu (1995). Moreover, the dynamic response of periodic cracks and randomly distributed cracks have been investigated by Zhang (1991) and Murai et al. (1995), respectively. Nevertheless, very few researches have been reported about the dynamic crack–hole interaction problems. Only very recently Liu and Liu (1999) analyzed the dynamic problem of two co-linear cracks located along the radial direction of a circular hole. As the Green's function of a half plane with a half circular hole is used in their paper, hence, the presented method in Liu and Liu (1999) is only valid for the case of co-linear cracks along radial direction. Due to the fact that the edge cracks generate more instability than ordinary cracks, there are many investigations concerning the dynamic edge cracks for a straight boundary (Liu et al., 1997; Stone et al., 1980; Datta and Shah, 1982; Abduljabbar et al., 1983). However, for arbitrary dynamic edge cracks of a circular boundary, no research has been carried out so far. Consequently, up to now, there does not exist general analytical method that can be used to solve the dynamic interaction between arbitrarily located cracks and a circular hole.

In principle, the finite element method (FEM) can be used to solve the dynamic crack–hole interaction problems. However, it requires the discretization of the entire volume around cracks and the hole. Also, for the unbounded domain, the absorbing boundary layers are necessary for the prevention of non-physical reflection from the calculation boundary. An alternative for solving the dynamic crack–hole interaction problems is the boundary element method (BEM). For the boundary element method, only the boundary of the calculation domain needs to be discretized. Moreover, for the unbounded domain, the non-reflecting condition can be satisfied automatically due to the analytical form of the Green's function. However, the direct application of the conventional displacement BEM equation to crack problems leads to ill-posed singular form displacement BEM equations (Cruse, 1988). Up to now, several numerical strategies have been developed to circumvent this limitation. One popular way of treating this problem is the multi-domain method in conjunction with the common displacement BEM equation (Lachat and Watson, 1976). The key point of the multi-domain method is to introduce artificial boundaries to make each region contain one crack surface. The two major disadvantages of the multi-domain method are the computational cost and the necessity of dealing with the singular stress field ahead of the crack. The displacement discontinuity method can also be used to solve the crack problem in the frame of BEM (Crouch and Starfield, 1983). A comprehensive discussion of the displacement discontinuity method can be found in Cruse (1996). Another option for dealing with the singular form problem is the dual boundary element method (DBEM). In the

DBEM, the singular form displacement BEM equation is avoided by using two different equations for the boundary nodes on the two opposite sides of the crack (Portela and Aliabadi, 1992; Selcuk et al., 1994). The obvious advantage of this method is it does not require any division of the calculation domain.

A drawback of the above-mentioned BEM for solving dynamic crack–hole interaction problems is the necessity of discretizing the circular-hole boundary numerically, which will reduce the accuracy. The objective of the present paper is to establish a special hypersingular integral equation method (HIEM) to analyze the interaction between arbitrarily located multiple cracks and a circular hole on the basis of the Green's function and the hypersingular integral equation method. The main difference between our approach and the BEM lies in using the crack opening displacements (COD) as the unknowns in our case, which can avoid the ill-posed BEM equation problem and will result in hypersingular integral equations for the CODs. Besides, the collocation method developed by Kaya and Erdogan is used to discretize the obtained hypersingular integral equations, which is different from the mesh discretization method used in the BEM. The hypersingular integral equation method (HIEM) has been used for the analysis of static crack problems for a long time (Ioakimidis, 1983; Chen, 1995; Kaya and Erdogan, 1987; Nied, 1987). For dynamic crack problems, there are also some researches have been done (Neerhoff, 1979; Krenk and Schmidt, 1982; van den Berg, 1981). The recent review concerning the elastic wave scattering by cracks has been presented by Boström (2003). The major advantages of the presented HIEM is that it can be used to calculate edge cracks of the circular hole due to the appropriate treatment of the Green's function. Moreover, due to the adoption of the specific Green's function for the circular boundary domain, our solution can satisfy the circular-hole boundary condition analytically. Consequently, in this sense, our approach in this paper belongs to a semi-analytical method. In order to develop our approach, the Green's function of a point harmonic antiplane force applied at an infinite plane containing a circular hole is derived by the Graf formula and the wave function expansion method. In terms of the asymptotic property of the Hankel function and the Bessel function, the Green's function is separated into a closed-form singular part and a regular part, which will facilitate the construction of hypersingular integral equations for the cracks. On the basis of the reciprocity principle as well as the obtained Green's function, the hypersingular boundary integral equations for the multiple cracks are derived. Numerical solution of the hypersingular integral equations yields the dynamic stress intensity factors (DSIF) at the crack tips. Comparison of our results with known results verifies the proposed method. For demonstration our method, some numerical results and corresponding discussions are given in the paper.

Summarizing, the contribution of the present paper are as follows: (1) the Green's function for a point force applied at an infinite plane containing a circular hole is derived, more importantly, the closed form expressions of the singular part Green's function are obtained for the first time; (2) the hypersingular boundary integral equations describing the dynamic interaction between the multiple cracks and a circular hole are established; (3) the dynamic stress intensity factors (DSIF) at the crack tips are calculated by the numerical solution of the obtained hypersingular integral equations.

2. Green's function

2.1. Derivation of the Green's function

In order to derive the hypersingular integral equations for the dynamic crack–hole interaction problem, the Green's function of a point harmonic force applied at an infinite plane with a circular hole is required. Here, the linear elastic infinite plane with a circular hole is assumed to be isotropic, the shear modulus and the density of which are μ, ρ, respectively. Suppose the radius of the circular hole is R. Without loss of generality, the origin of the coordinate system xoy is assumed to coincide with the center of the circular hole (Fig. 1).

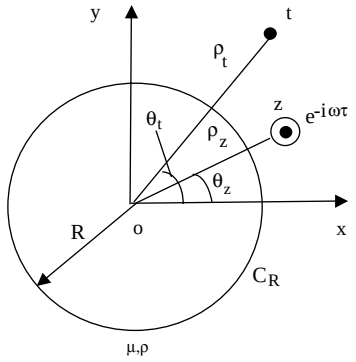

Fig. 1. An infinite plane with a circular hole and subject to a harmonic point antiplane force.

The Green's function of the point force consists of two parts: a principal part and a complementary part. The principal part is the solution for a point harmonic force applied at an infinite homogenous plane without circular hole, while the complementary part is the scattered field of the circular hole due to the incident wave of the principal Green's function, which can be determined using wave function expansion method as well as the boundary condition along the hole surface.

Suppose the point force is applied at point $z = \rho_z e^{i\theta_z}$, where ρ_z, θ_z denote the polar distance and polar angle and $i = \sqrt{-1}$ (Fig. 1). The longitudinal displacement for the principal Green's function has the form (Achenbach, 1973)

$$w^{G^{(p)}}(t,z) = \frac{i}{4\mu} H_0^{(1)}(k|t-z|)\, e^{-i\omega\tau} \tag{1}$$

$t = \rho_t e^{i\theta_t}$ is the receiver, the superscript $G^{(p)}$ denotes the principal Green's function, $k = \omega/v_s$ is the wave number and ω, v_s are angular frequency and shear wave velocity and $H_0^{(1)}(\bullet)$ denotes the zero order Hankel function of the first kind. Since all the physical quantities contain the common time factor $e^{-i\omega\tau}$, for simplicity, it will be omitted in the remainder of the paper.

By using the Graf formula (Watson, 1962), the longitudinal displacement (1) is recast in the following form

$$w^{G^{(p)}}(t,z) = \frac{i}{4\mu} \sum_{m=0}^{\infty} \varepsilon_m J_m(k\rho_t) H_m^{(1)}(k\rho_z) \cos[m(\theta_t - \theta_z)], \quad \rho_t < \rho_z \tag{2a}$$

$$w^{G^{(p)}}(t,z) = \frac{i}{4\mu} \sum_{m=0}^{\infty} \varepsilon_m J_m(k\rho_z) H_m^{(1)}(k\rho_t) \cos[m(\theta_t - \theta_z)], \quad \rho_z < \rho_t \tag{2b}$$

where $J_m(\bullet)$ is the mth order first kind Bessel function; $\varepsilon_m = 1$ if $m = 0$, $\varepsilon_m = 2$ if $m \geqslant 1$ and in the remainder of the paper, ε_m has the same value.

Using the constitutive relations of the infinite plane, the stresses for the principal Green's function are

$$\sigma_{zr}^{G^{(p)}}(t,z) = \frac{ik}{4} \sum_{m=0}^{\infty} \varepsilon_m J_m'(k\rho_t) H_m^{(1)}(k\rho_z) \cos[m(\theta_t - \theta_z)], \quad \rho_t < \rho_z \tag{3a}$$

$$\sigma_{z\theta}^{G^{(p)}}(t,z) = -\frac{i}{4\rho_t} \sum_{m=1}^{\infty} m\varepsilon_m J_m(k\rho_t) H_m^{(1)}(k\rho_z) \sin[m(\theta_t - \theta_z)], \quad \rho_t < \rho_z \tag{3b}$$

$$\sigma_{zr}^{G^{(p)}}(t,z) = \frac{ik}{4}\sum_{m=0}^{\infty}\varepsilon_m J_m(k\rho_z)H_m^{(1)'}(k\rho_t)\cos[m(\theta_t-\theta_z)], \quad \rho_z < \rho_t \tag{3c}$$

$$\sigma_{z\theta}^{G^{(p)}}(t,z) = -\frac{i}{4\rho_t}\sum_{m=1}^{\infty} m\varepsilon_m J_m(k\rho_z)H_m^{(1)}(k\rho_t)\sin[m(\theta_t-\theta_z)], \quad \rho_z < \rho_t \tag{3d}$$

where a prime denotes derivative with respect to the corresponding variable. In terms of the wave function expansion method (Pao and Mow, 1973), the complementary Green's function, i.e., the scattered field of the circular hole due to the incident wave (1) may be expressed by

$$w^{G^{(d)}}(t,z) = \sum_{m=0}^{\infty} A_m H_m^{(1)}(k\rho_t)\cos[m(\theta_t-\theta_z)] \tag{4}$$

where the superscript $G^{(d)}$ denotes the complementary Green's function. In terms of (1), (3) and (4), the displacement and stresses of the total Green's function are given by the following expressions

$$w^{G}(t,z) = w^{G^{(p)}}(t,z) + w^{G^{(d)}}(t,z) \tag{5a}$$

$$\sigma_{zr}^{G}(t,z) = \sigma_{zr}^{G^{(p)}}(t,z) + \sigma_{zr}^{G^{(d)}}(t,z) \tag{5b}$$

$$\sigma_{z\theta}^{G}(t,z) = \sigma_{z\theta}^{G^{(p)}}(t,z) + \sigma_{z\theta}^{G^{(d)}}(t,z) \tag{5c}$$

The total Green's function satisfies following stress boundary condition

$$\mu\frac{\partial[w^{G^{(p)}}(t,z) + w^{G^{(d)}}(t,z)]}{\partial\rho_t}\bigg|_{\rho_t=R} = 0 \tag{6}$$

Inserting Eqs. (2a), (4) into (6), the coefficients A_m in Eq. (4) are obtained

$$A_m = -\frac{i\varepsilon_m}{4\mu}\frac{H_m^{(1)}(k\rho_z)J_m'(kR)}{H_m^{(1)'}(kR)} \tag{7}$$

Substituting Eq. (7) into Eq. (4) and using Eqs. (2) and (5), the total Green's function can be obtained.

In terms of the constitutive relations, the stresses for the complementary Green's function in Eq. (5b) and (5c) have the following expressions

$$\sigma_{zr}^{G^{(d)}}(t,z) = \mu k\sum_{m=0}^{\infty} A_m H_m^{(1)'}(k\rho_t)\cos[m(\theta_t-\theta_z)] \tag{8a}$$

$$\sigma_{z\theta}^{G^{(d)}}(t,z) = -\frac{\mu}{\rho_t}\sum_{m=1}^{\infty} mA_m H_m^{(1)}(k\rho_t)\sin[m(\theta_t-\theta_z)] \tag{8b}$$

where coefficients A_m are given by Eq. (7).

2.2. The decomposition of the Green's function

In the previous section, the Green's function of a point force was determined. It follows from Eq. (1) that the principal Green's function is unbounded when $t \to z$. In order to establish the hypersingular integral equations for the cracks as well as to calculate the Green's function correctly, the singular parts should be extracted from the total Green's function.

The procedure of extracting singular part from Eq. (3) consists in subtracting the divergent parts from the series of the Green's function and calculating the closed form expressions for the divergent parts. In order to explain the decomposition procedure, we take Eq. (3a) as an example.

Hankel function and Bessel function of the first kind have the following asymptotic property (Abramowitz and Stegun, 1965)

$$H_m^{(1)}(\xi) \to -\frac{(m-1)!}{\pi}\left(\frac{2}{\xi}\right)^m i, \quad (m \to \infty) \tag{9a}$$

$$J_m(\xi) \to \frac{1}{m!}\left(\frac{\xi}{2}\right)^m, \quad (m \to \infty) \tag{9b}$$

Using Eq. (9), Eq. (3a) is rewritten as

$$\begin{aligned}\sigma_{zr}^{G^{(p)}}(t,z) = &\sum_{m=1}^{\infty}\left[\frac{ik}{2}J_m'(k\rho_t)H_m^{(1)}(k\rho_z) - \frac{1}{2\pi\rho_t}\left(\frac{\rho_t}{\rho_z}\right)^m\right]\cos[m(\theta_t-\theta_z)] + \frac{ik}{4}J_0'(k\rho_t)H_0^{(1)}(k\rho_z)\\ &+\sum_{m=1}^{\infty}\frac{1}{2\pi\rho_t}\left(\frac{\rho_t}{\rho_z}\right)^m\cos[m(\theta_t-\theta_z)], \quad \rho_t < \rho_z\end{aligned} \tag{10}$$

The first and the second term in Eq. (10) are everywhere finite, while the third term in the above equation is unbounded when $t \to z$. However, the closed form expression for the third term has the form

$$\begin{aligned}&\sum_{m=1}^{\infty}\frac{1}{2\pi\rho_t}\left(\frac{\rho_t}{\rho_z}\right)^m\cos[m(\theta_t-\theta_z)]\\ &\quad=\frac{1}{4\pi\rho_t}\sum_{m=1}^{\infty}\left\{\left[\frac{\rho_t}{\rho_z}e^{i(\theta_t-\theta_z)}\right]^m+\left[\frac{\rho_t}{\rho_z}e^{-i(\theta_t-\theta_z)}\right]^m\right\}=\frac{1}{4\pi}\left(\frac{e^{i\theta_t}}{z-t}+\frac{e^{-i\theta_t}}{\bar{z}-\bar{t}}\right), \quad \rho_t<\rho_z\end{aligned} \tag{11}$$

where $\bar{z} = \rho_z e^{-i\theta_z}$ and $\bar{t} = \rho_t e^{-i\theta_t}$ denote the complex conjugates of z and t, respectively.

Therefore, it follows from (10) and (11) that the Green's function of Eq. (10) has been divided into a singular part and a bounded part. The singular part has a closed form expression and becomes unbounded when $t \to z$, while the bounded part is everywhere finite. Eq. (3b) can have similar decomposition if the same decomposition method is used. Consequently, the stresses of the principal Green's function for $\rho_t < \rho$ have following decomposition

$$\sigma_{zr}^{G^{(p)}}(t,z) = \sigma_{zrR}^{G^{(p)}}(t,z) + \sigma_{zrS}^{G^{(p)}}(t,z) \tag{12a}$$

$$\sigma_{z\theta}^{G^{(p)}}(t,z) = \sigma_{z\theta R}^{G^{(p)}}(t,z) + \sigma_{z\theta S}^{G^{(p)}}(t,z) \tag{12b}$$

where the subscripts R and S represent the regular and singular part of the Green's function and the regular and the singular stresses are given by

$$\sigma_{zrR}^{G^{(p)}}(t,z) = \sum_{m=1}^{\infty}\left[\frac{ik}{2}J_m'(k\rho_t)H_m^{(1)}(k\rho_z) - \frac{1}{2\pi\rho_t}\left(\frac{\rho_t}{\rho_z}\right)^m\right]\cos[m(\theta_t-\theta_z)] + \frac{ik}{4}J_0'(k\rho_t)H_0^{(1)}(k\rho_z), \quad \rho_t<\rho_z \tag{13a}$$

$$\sigma_{zrS}^{G^{(p)}}(t,z) = \frac{1}{4\pi}\left(\frac{e^{i\theta_t}}{z-t}+\frac{e^{-i\theta_t}}{\bar{z}-\bar{t}}\right), \quad \rho_t<\rho_z \tag{13b}$$

$$\sigma_{z\theta R}^{G^{(p)}}(t,z) = -\sum_{m=1}^{\infty}\left[\frac{i}{2\rho_t} m J_m(k\rho_t) H_m^{(1)}(k\rho_z) - \frac{1}{2\pi\rho_t}\left(\frac{\rho_t}{\rho_z}\right)^m\right]\sin[m(\theta_t-\theta_z)], \quad \rho_t < \rho_z \tag{13c}$$

$$\sigma_{z\theta S}^{G^{(p)}}(t,z) = -\frac{1}{4\pi i}\left(\frac{e^{i\theta_t}}{z-t} - \frac{e^{-i\theta_t}}{\bar{z}-\bar{t}}\right), \quad \rho_t < \rho_z \tag{13d}$$

Similarly, for the case of $\rho_t > \rho_z$ in Eqs. (3c) and (3d), using the same decomposition method as above, one has the same decomposition formula as Eq. (12). The corresponding regular part and the singular part stresses for Eqs. (3c) and (3d) are given by

$$\sigma_{zrR}^{G^{(p)}}(t,z) = \sum_{m=0}^{\infty}\left[\frac{ik\varepsilon_m}{4} J_m(k\rho_z) H_m^{(1)'}(k\rho_t) + \frac{1}{2\pi\rho_t}\left(\frac{\rho_z}{\rho_t}\right)^m\right]\cos[m(\theta_t-\theta_z)], \quad \rho_t > \rho_z \tag{14a}$$

$$\sigma_{zrS}^{G^{(p)}}(t,z) = \frac{1}{4\pi}\left(\frac{e^{i\theta_t}}{z-t} + \frac{e^{-i\theta_t}}{\bar{z}-\bar{t}}\right), \quad \rho_t > \rho_z \tag{14b}$$

$$\sigma_{z\theta R}^{G^{(p)}}(t,z) = -\sum_{m=1}^{\infty}\left[\frac{i}{2\rho_t} m J_m(k\rho_z) H_m^{(1)}(k\rho_t) - \frac{1}{2\pi\rho_t}\left(\frac{\rho_z}{\rho_t}\right)^m\right]\sin[m(\theta_t-\theta_z)], \quad \rho_t > \rho_z \tag{14c}$$

$$\sigma_{z\theta S}^{G^{(p)}}(t,z) = -\frac{1}{4\pi i}\left(\frac{e^{i\theta_t}}{z-t} - \frac{e^{-i\theta_t}}{\bar{z}-\bar{t}}\right), \quad \rho_t > \rho_z \tag{14d}$$

From Eqs. (13) and (14), it can be seen that the singular stresses of the principal Green's function have the same expressions for the case of $\rho_t < \rho_z$ and $\rho_t > \rho_z$. Therefore, in global Cartesian coordinates xoy, the singular stresses of the principal Green's function have the following uniform expression

$$\sigma_{zxS}^{G^{(p)}}(t,z) - i\sigma_{zyS}^{G^{(p)}}(t,z) = \frac{1}{2\pi}\frac{1}{z-t} \tag{15}$$

Note that except for the time factor $e^{-i\omega\tau}$, the singular stresses of the principal Green's function coincide with the Green's function of the corresponding static problem.

On the other hand, it follows from Eqs. (7)–(9) that if $z \to C_R$ and $t \to z$, the complementary Green's function given by Eqs. (7) and (8) are unbounded. Consequently, the complementary Green's function also contains singular parts. For the same reason, the singular parts must be subtracted from the complementary Green's function. We shall use Eq. (8a) to explain the decomposition of the complementary Green's function. Using Eqs. (7) and (9), Eq. (8a) is separated as follows

$$\begin{aligned}\sigma_{zr}^{G^{(d)}}(t,z) = &\sum_{m=1}^{\infty}\left[\mu k A_m H_m^{(1)'}(k\rho_t) + \frac{1}{2\pi}\frac{1}{\rho_t}\left(\frac{R^2}{\rho_t\rho_z}\right)^m\right]\cos[m(\theta_t-\theta_z)] + \mu k A_0 H_0^{(1)'}(k\rho_t)\\ &-\sum_{m=1}^{\infty}\frac{1}{2\pi}\frac{1}{\rho_t}\left(\frac{R^2}{\rho_t\rho_z}\right)^m\cos[m(\theta_t-\theta_z)]\end{aligned} \tag{16}$$

where the first and second terms in the above equation are bounded while the third term is unbounded when $z \to C_R$ and $t \to z$. The closed form expression for the third term has the form

$$\begin{aligned}-\sum_{m=1}^{\infty}\frac{1}{2\pi}\frac{1}{\rho_t}\left(\frac{R^2}{\rho_t\rho_z}\right)^m\cos[m(\theta_t-\theta_z)] &= -\frac{1}{4\pi\rho_t}\sum_{m=1}^{\infty}\left\{\left[\frac{R^2}{\rho_t\rho_z}e^{i(\theta_t-\theta_z)}\right]^m + \left[\frac{R^2}{\rho_t\rho_z}e^{-i(\theta_t-\theta_z)}\right]^m\right\}\\ &= -\frac{1}{4\pi}\frac{1}{t}\left(\frac{R^2e^{i\theta_t}}{\bar{t}z-R^2} + \frac{R^2e^{i\theta_t}}{t\bar{z}-R^2}\right)\end{aligned} \tag{17}$$

Using Eqs. (7) and (9), Eq. (8b) can be separated in a similar way. Consequently, the stresses of the complementary Green's function have the following decomposition

$$\sigma_{zr}^{G^{(d)}}(t,z) = \sigma_{zrR}^{G^{(d)}}(t,z) + \sigma_{zrS}^{G^{(d)}}(t,z) \tag{18a}$$

$$\sigma_{z\theta}^{G^{(d)}}(t,z) = \sigma_{z\theta R}^{G^{(d)}}(t,z) + \sigma_{z\theta S}^{G^{(d)}}(t,z) \tag{18b}$$

where the regular and singular stresses are given by

$$\sigma_{zrR}^{G^{(d)}}(t,z) = \sum_{m=1}^{\infty}\left[\mu k A_m H_m^{(1)'}(k\rho_t) + \frac{1}{2\pi}\frac{1}{\rho_t}\left(\frac{R^2}{\rho_t\rho_z}\right)^m\right]\cos[m(\theta_t-\theta_z)] + \mu k A_0 H_0^{(1)'}(k\rho_t) \tag{19a}$$

$$\sigma_{zrS}^{G^{(d)}}(t,z) = -\frac{1}{4\pi}\frac{1}{t}\left(\frac{R^2 e^{i\theta_t}}{\bar{t}z-R^2} + \frac{R^2 e^{i\theta_t}}{t\bar{z}-R^2}\right) \tag{19b}$$

$$\sigma_{z\theta R}^{G^{(d)}}(t,z) = -\sum_{m=1}^{\infty}\left[\frac{\mu}{\rho_t} m A_m H_m^{(1)}(k\rho_t) - \frac{1}{2\pi}\frac{1}{\rho_t}\left(\frac{R^2}{\rho_t\rho_z}\right)^m\right]\sin[m(\theta_t-\theta_z)] \tag{19c}$$

$$\sigma_{z\theta S}^{G^{(d)}}(t,z) = -\frac{1}{4\pi i}\frac{1}{t}\left(\frac{R^2 e^{i\theta_t}}{\bar{t}z-R^2} - \frac{R^2 e^{i\theta_t}}{t\bar{z}-R^2}\right) \tag{19d}$$

where the coefficients A_m are given by Eq. (7).

If the following stress combination is introduced, the singular stresses in Eq. (19) is rewritten as

$$\sigma_{zxS}^{G^{(d)}}(t,z) - i\sigma_{zyS}^{G^{(d)}}(t,z) = -\frac{1}{2\pi}\frac{R^2}{t(\bar{t}z-R^2)} \tag{20}$$

It is worth noting that the singular stresses of the complementary Green's function in Eq. (20) have the same expressions as the corresponding static case except the time factor $e^{-i\omega\tau}$ (Lu, 2000).

In this section, the Green's function of a point harmonic force applied at an infinite plane with a circular hole is derived. The Green's function is separated into a regular part and singular part. The closed form expressions for the singular part Green's function, which are crucial for the construction of the hypersingular integral equations, are obtained for the first time.

3. The hypersingular boundary integral equations for the multiple cracks

The total wave fields of the crack–hole interaction problem can be divided into two parts. One part is the free field, in which case it is assumed that the cracks do not exist. Then, the free wave field is determined by the incident plane SH wave and the scattered field of the circular hole. The scattered field of the circular hole can be obtained by using the wave function expansion method. The other part is the scattered field of the cracks. On the basis of the reciprocity principle and using the obtained Green's function, the scattered field of the cracks can be expressed by the crack opening displacements (COD). Using the boundary conditions along the crack surfaces, the hypersingular integral equations can be obtained in terms of the free wave field and the scattered field of the cracks.

3.1. The scattered field of a single crack

Suppose there are N arbitrarily located cracks near a circular hole (Fig. 2). The total scattered field of the N cracks is the superposition of the scattered fields of the N single cracks; hence in order to obtain the total scattered field, the scattered field of a single crack is required.

Assume that the half length of crack L_j is a_j and the two tips of the crack are A_j, B_j, respectively. The obliquity angle of L_j with respect to the x-axis is $\alpha_j + \beta_j$; the polar angle and polar distance of tip A_j are α_j, ρ_{A_j} respectively; the obliquity angle of L_j with respect to the x_j-axis is β_j (Fig. 2). Since the Green's function has been separated into a singular and a regular part, accordingly, the scattered field of the L_j can also be divided into a singular part and a regular part.

To begin with, we discuss the singular scattered field of the L_j. Let the crack opening displacement (COD) of L_j be $\Psi_j(u)$, $0 \leqslant u \leqslant 2a_j$ (Fig. 2). By using Eqs. (15) and (20) and the reciprocity principle (Kupradze, 1965), the displacement of the singular scattered field of the crack L_j is obtained as follows

$$w_S^{(s_j)}(z) = -\frac{1}{4\pi i}\int_0^{2a_j} \Psi_j(u)\left[\frac{\mathrm{e}^{\mathrm{i}(\alpha_j+\beta_j)}}{z-t} - \frac{\mathrm{e}^{-\mathrm{i}(\alpha_j+\beta_j)}}{\bar{z}-\bar{t}}\right]\mathrm{d}u + \frac{1}{4\pi i}\int_0^{2a_j} \Psi_j(u)\left[\frac{R^2\mathrm{e}^{\mathrm{i}(\alpha_j+\beta_j)}}{t(t\bar{z}-R^2)} - \frac{R^2\mathrm{e}^{-\mathrm{i}(\alpha_j+\beta_j)}}{\bar{t}(\bar{t}z-R^2)}\right]\mathrm{d}u \tag{21}$$

where the superscript s_j represents the scattered field of the crack L_j; the subscript S denotes the singular part of the scattered field; $z = \rho_z \mathrm{e}^{i\theta_z} = x + \mathrm{i}y$, t is integration point and $t = \rho_t \mathrm{e}^{\mathrm{i}\theta_t} = \rho_{A_j}\mathrm{e}^{i\alpha_j} + u\mathrm{e}^{\mathrm{i}(\alpha_j+\beta_j)}$. Using the constitutive relation, the stress of the singular scattered field of the crack L_j in xoy–coordinate system are given by

$$\sigma_{zxS}^{(s_j)}(z) - \mathrm{i}\sigma_{zyS}^{(s_j)}(z) = \frac{\mu}{2\pi i}\int_0^{2a_j} \Psi_j(u)\frac{\mathrm{e}^{\mathrm{i}(\alpha_j+\beta_j)}}{(t-z)^2}\,\mathrm{d}u + \frac{\mu}{2\pi i}\int_0^{2a_j} \Psi_j(u)\frac{R^2\mathrm{e}^{-\mathrm{i}(\alpha_j+\beta_j)}}{(\bar{t}z-R^2)^2}\,\mathrm{d}u \tag{22}$$

The regular scattered field of the L_j can also be obtained by using the regular Green's function (13), (14) and (19) as well as the reciprocity principle (Kupradze, 1965). The longitudinal displacement of the regular scattered field of the L_j reads

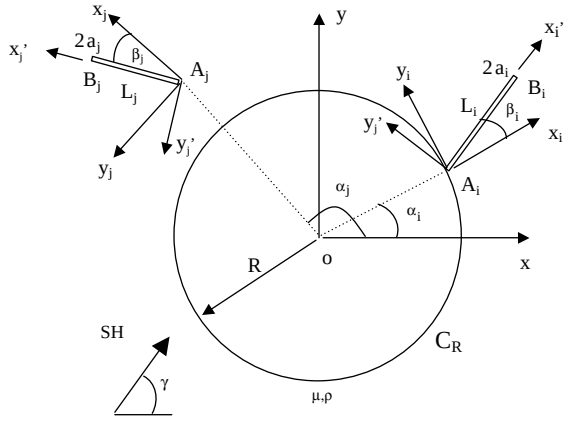

Fig. 2. Dynamic interaction between multiple cracks and a circular hole swept by SH wave.

$$w_R^{(s_j)}(z)=\int_0^{2a_j}\Psi_j(u)\Big\{[\sigma_{z0R}^{G^{(p)}}(t,z)+\sigma_{z0R}^{G^{(d)}}(t,z)]\cos(\alpha_j+\beta_j-\theta_t)-\Big[\sigma_{zrR}^{G^{(p)}}(t,z)+\sigma_{zrR}^{G^{(d)}}(t,z)\Big]\sin(\alpha_j+\beta_j-\theta_t)\Big\}\mathrm{d}u \tag{23}$$

where the subscript R in (23) represents the regular part of the scattered field and the stress components $\sigma_{z\theta R}^{G^{(p)}}(t,z)$, $\sigma_{z\theta R}^{G^{(d)}}(t,z)$, $\sigma_{zrR}^{G^{(p)}}(t,z)$, $\sigma_{zrR}^{G^{(d)}}(t,z)$ in Eq. (23) are given by Eqs. (13), (14) and (19). The stresses determined by the regular scattered field of L_j have the form

$$\sigma_{zrR}^{(s_j)}(z)=\mu\int_0^{2a_j}\Psi_j(u)\Bigg\{\left[\frac{\partial\sigma_{z\theta R}^{G^{(p)}}(t,z)}{\partial\rho_z}+\frac{\partial\sigma_{z\theta R}^{G^{(d)}}(t,z)}{\partial\rho_z}\right]\cos(\alpha_j+\beta_j-\theta_t)-\left[\frac{\partial\sigma_{zrR}^{G^{(p)}}(t,z)}{\partial\rho_z}+\frac{\partial\sigma_{zrR}^{G^{(d)}}(t,z)}{\partial\rho_z}\right]\times\sin(\alpha_j+\beta_j-\theta_t)\Bigg\}\mathrm{d}u \tag{24a}$$

$$\sigma_{z\theta R}^{(s_j)}(z)=\frac{\mu}{\rho_z}\int_0^{2a_j}\Psi_j(u)\Bigg\{\left[\frac{\partial\sigma_{z\theta R}^{G^{(p)}}(t,z)}{\partial\theta_z}+\frac{\partial\sigma_{z\theta R}^{G^{(d)}}(t,z)}{\partial\theta_z}\right]\cos(\alpha_j+\beta_j-\theta_t)-\left[\frac{\partial\sigma_{zrR}^{G^{(p)}}(t,z)}{\partial\theta_z}+\frac{\partial\sigma_{zrR}^{G^{(d)}}(t,z)}{\partial\theta_z}\right]\times\sin(\alpha_j+\beta_j-\theta_t)\Bigg\}\mathrm{d}u \tag{24b}$$

3.2. Derivation of the hypersingular boundary integral equations

The considerations of the above section gave us the scattered field of a single crack. The total scattered field of the N cracks can be obtained by superposing the scattered fields of the N single cracks. As mentioned above, the hypersingular integral equations can be constructed by using the free wave field and the total scattered field of the N cracks. The superposition of the free wave field and the scattered field of the cracks satisfies the stress-free condition along the crack surfaces. Consequently, for an arbitrary collocation point z (Fig. 2) at the crack L_i, one has

$$\sigma_{zy_i'}^{(f)}(z)+\sum_{j=1}^{N}\sigma_{zy_i'}^{(s_j)}(z)=0,\quad z\in L_i,\quad i=1,\ldots,N \tag{25}$$

where the superscript f denotes the free wave field and the subscript zy_i' of the stresses implies that the stresses in Eq. (25) are the stress components with respect to the $x_i'A_iy_i'$ coordinate system (Fig. 2). Substitution of Eqs. (22) and (24) into (25) yields the following group of hypersingular integral equations for the multiple cracks

$$\frac{\mu}{2\pi}\ \text{f.p.}\int_0^{2a_i}\frac{\Psi_i(u)}{(u-v)^2}\mathrm{d}u+\frac{\mu}{2\pi}\int_0^{2a_i}\Psi_i(u)Re\left[\frac{R^2}{(\bar{t}z-R^2)^2}\right]\mathrm{d}u+\sum_{j=1}^{N(j\neq i)}\int_0^{2a_j}\Psi_j(u)k_{ijS}(t,z)\,\mathrm{d}u+\sum_{j=1}^{N}\int_0^{2a_j}\Psi_j(u)k_{ijR}(t,z)\,\mathrm{d}u=-\sigma_{zy_i'}^{(f)}(z) \tag{26a}$$

$$0\leqslant v\leqslant 2a_i,\quad z\in L_i,\ i=1,\ldots,N,\quad 0\leqslant u\leqslant 2a_j,\ j=1,\ldots,N$$

$$k_{ijS}(t,z)=\frac{\mu}{2\pi}Re\left[\frac{\mathrm{e}^{\mathrm{i}(\alpha_i+\beta_i+\alpha_j+\beta_j)}}{(t-z)^2}\right]+\frac{\mu}{2\pi}Re\left[\frac{R^2\mathrm{e}^{\mathrm{i}(\alpha_i+\beta_i-\alpha_j-\beta_j)}}{(\bar{t}z-R^2)^2}\right] \tag{26b}$$

$$k_{ijR}(t,z)=\frac{\mu}{\rho_z}\left[\frac{\partial\sigma_{z\theta R}^{G^{(p)}}(t,z)}{\partial\theta_z}+\frac{\partial\sigma_{z\theta R}^{G^{(d)}}(t,z)}{\partial\theta_z}\right]\cos(\alpha_j+\beta_j-\theta_t)\cos(\alpha_i+\beta_i-\theta_z)-\frac{\mu}{\rho_z}\left[\frac{\partial\sigma_{zrR}^{G^{(p)}}(t,z)}{\partial\theta_z}+\frac{\partial\sigma_{zrR}^{G^{(d)}}(t,z)}{\partial\theta_z}\right]$$
$$\times\sin(\alpha_j+\beta_j-\theta_t)\cos(\alpha_i+\beta_i-\theta_z)-\mu\left[\frac{\partial\sigma_{z\theta R}^{G^{(p)}}(t,z)}{\partial\rho_z}+\frac{\partial\sigma_{z\theta R}^{G^{(d)}}(t,z)}{\partial\rho_z}\right]\cos(\alpha_j+\beta_j-\theta_t)$$
$$\times\sin(\alpha_i+\beta_i-\theta_z)+\mu\left[\frac{\partial\sigma_{zrR}^{G^{(p)}}(t,z)}{\partial\rho_z}+\frac{\partial\sigma_{zrR}^{G^{(d)}}(t,z)}{\partial\rho_z}\right]\sin(\alpha_j+\beta_j-\theta_t)\sin(\alpha_i+\beta_i-\theta_z) \tag{26c}$$

where f.p. indicates that the hypersingular integral in the above equations must be defined in the sense of a finite-part integral (Hadamard, 1923); $z=\rho_z e^{i\theta_z}=\rho_{A_i}e^{i\alpha_i}+ve^{i(\alpha_i+\beta_i)}$ is the collocation point on L_i and $t=\rho_t e^{i\theta_t}=\rho_{A_j}e^{i\alpha_j}+ue^{i(\alpha_j+\beta_j)}$ is the integration point located on L_j.

4. Numerical method and results

4.1. Numerical method for solving the hypersingular integral equations

The integral equation (26) are one-dimensional hypersingular integral equations. There is a standard numerical method for solving this kind of hypersingular integral equation (Kaya and Erdogan, 1987). Before numerical solution, we standardize the above hypersingular integral equations as follows

$$\frac{\mu}{2\pi}\ \text{f.p.}\int_{-1}^{1}\frac{\psi_i(\tau)\,d\tau}{(\tau-r)^2}+\frac{\mu}{2\pi}\int_{-1}^{1}\psi(\tau)\,d\tau Re\left\{\frac{R^2a_i^2}{[\bar{t}(\tau)z(r)-R^2]^2}\right\}+\sum_{j=1}^{N(j\neq i)}\int_{-1}^{+1}\psi_j(\tau)k_{ijS}[t(\tau),z(r)]a_j^2\,d\tau$$
$$+\sum_{j=1}^{N}\int_{-1}^{+1}\psi_j(\tau)k_{ijR}[t(\tau),z(r)]a_j^2\,d\tau=-\sigma_{zy_i'}^{(f)}[z(r)],z(r)\in L_i,\quad i=1,\ldots,N \tag{27}$$

where $\tau=(u-a_j)/a_j,\quad j=1,\ldots,N,\quad r=(v-a_i)/a_i,\quad i=1,\ldots,N,\quad -1\leqslant\tau,\ r\leqslant+1,\quad \psi_i(\tau)=\frac{1}{a_i}\Psi_i(u),\ i=1,\ldots,N.$

The unknown functions in Eq. (27) are assumed following form

$$\psi_i(\tau)=(1+\tau)^{\gamma_i}(1-\tau)^{1/2}h_i(\tau),\quad h_i(\tau)=\sum_{k=0}^{M}c_{ik}\tau^k \tag{28a, b}$$

where γ_i and 1/2 are the stress singularity order at the tip A_i and B_i; $h_i(\tau)$ are analytical functions which are expanded into Taylor series (28b). In the present paper, we truncate the series and take M terms to approximate the functions $h_i(\tau)$. Our calculations demonstrate that if M is larger than 6, satisfactory results can be achieved. Note that generally, for the dynamic problem in this paper, the coefficients c_{ik} in Eq. (28b) are complex.

The γ_i in Eq. (28a) takes the value 1/2 if the tip A_i is embedded in the homogeneous linear elastic medium, while it vanishes if the tip A_i terminates at the boundary of the circular hole (Kaya and Erdogan, 1987).

For calculating the hypersingular integral in the integral equations, following finite-part regularization formula (Hadamard, 1923; Kaya and Erdogan, 1987) is used

$$\text{f.p.}\int_{-1}^{1}\frac{\psi(\tau)\,d\tau}{(\tau-r)^2}=\int_{-1}^{1}[\psi(\tau)-\psi(r)-(\tau-r)\psi'(r)]\frac{d\tau}{(\tau-r)^2}-\psi(r)\left(\frac{1}{1+r}+\frac{1}{1-r}\right)+\psi'(r)\log\left(\frac{1-r}{1+r}\right) \tag{29}$$

where the integral on right-hand side is a convergent improper integral.

If the collocation points for discretization of Eq. (27) are chosen according to the formula

$$r_k = \cos\left(\frac{2k+1}{M+1}\frac{\pi}{2}\right) \quad (k = 0, 1, \ldots, M) \tag{30}$$

Eq. (27) can be reduced to $(M+1)\times N$ complex algebraic equations. Numerical solution of the $(M+1)\times N$ complex algebraic equations yields the complex coefficients in Eq. (28b). The functions $h_i(\tau_i)$ and the dynamic stress intensity factors (DSIF) at the crack tips can be calculated in a straightforward manner after determining the complex coefficients.

As mentioned above, if the tip A_i terminates at the hole boundary, there is no stress singularity at the tip A_i. If tip A_i is embedded in the homogeneous linear elastic medium, then in a neighborhood of the tip A_i $(u = 0)$, the crack open displacement (COD) $\Psi_i(u)$ of the crack L_i has the form

$$\Psi_i(u) = u^{1/2}\Psi^*_{A_i}(u) \tag{31}$$

where $\Psi^*_{A_i}(u)$ satisfies the Hölder condition in a neighborhood of the tip A_i. By using the behavior of Cauchy type integral (Muskhelishvili, 1953a), the dynamic stress intensity factor (DSIF) of the tip A_i is expressed as

$$K_{3A_i} = \frac{\sqrt{2\pi}}{4}\mu\Psi^*_{A_i}(0) \tag{32}$$

Similarly, at the neighborhoods of tip B_i $(u = 2a_i)$, the crack open displacement (COD) $\Psi_i(u)$ has the form

$$\Psi_i(u) = (2a_i - u)^{1/2}\Psi^*_{B_i}(u) \tag{33}$$

where $\Psi^*_{B_i}(u)$ satisfies the Hölder condition in the neighborhoods of the tip B_i. Again, by the asymptotic property of Cauchy type integral (Muskhelishvili, 1953a), the dynamic stress intensity factor (DSIF) at the tip B_i is given by the expression

$$K_{3B_i} = \frac{\sqrt{2\pi}}{4}\mu\Psi^*_{B_i}(2a_i) \tag{34}$$

4.2. Numerical results and discussion

Although the present method is quite general, due to the limitations of the paper, we only present calculation and discussion for some typical examples. For verifying the proposed method, in Section 4.2.1. our results are compared with some known results. In Sections 4.2.2–4.2.6 some numerical results and corresponding analysis are given. In computation, the Green's functions in Eqs. (13),(14) and (19) are expressed as 50-term truncated series. The parameter M in Eq. (28b) is taken as 8 in all the numerical examples.

4.2.1. Comparison of our results with known results

In this section, some special cases of our solution are compared with three known results. The comparison shows that our solution is in a good agreement with the known results.

Two co-linear radial cracks of the same length terminate at opposite sides of the boundary of a circular hole. If the length of the cracks is much larger than the radius of the circular hole, then the crack–hole interaction problem is reduced to a single straight crack problem. In calculation, let $a_1 = a_2 = 0.5$, $R = 0.01$ and the incidence angle of SH wave equal to 90°. The results (DSIF) of present paper are compared with Fig. 2 in Loeber and Sih (1968). From Fig. 3, it can be seen that our results agree very well with those of Loeber and Sih (1968).

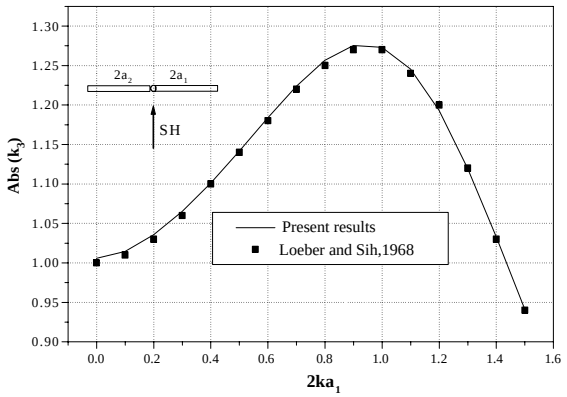

Fig. 3. Results of this paper for the case of two co-linear edge cracks with the hole radius tending to zero compared with those of Loeber and Sih (1968).

Two co-linear radial cracks of the same length terminate at the opposite sides of the boundary of a circular hole. The incidence angle of SH wave is 90°. This particular problem was solved in Liu and Liu (1999). The comparison of the results (DSIF) of the present paper with those of Liu and Liu (1999) is shown in Fig. 4. It can be seen clearly from Fig. 4 that the present results are in good agreement with those of Liu and Liu (1999).

The incidence angle of SH wave is 90°. If let the wave number of the incident wave approach zero, then, the dynamic problem in this paper is reduced to a static crack–hole interaction problem. The position of the two cracks are shown in Fig. 5. Our results are compared with those of Chen and Wang (1986). From Table 1, an extremely good agreement between the two results is observed.

4.2.2. The influence of the length of an edge crack on its DSIFs

In this example, the relation between the length of an edge crack and its DSIFs will be considered. The two tips of the crack are A and B, respectively. The tip A of the crack terminates at the boundary of the circular hole, while the tip B of the crack is located in the homogeneous medium. Therefore, one has $\rho_A = R$. The length of the crack is $2a$ and the ratio a/R takes $0.1, 0.3, 0.7, 1.0$. In calculation, we assume

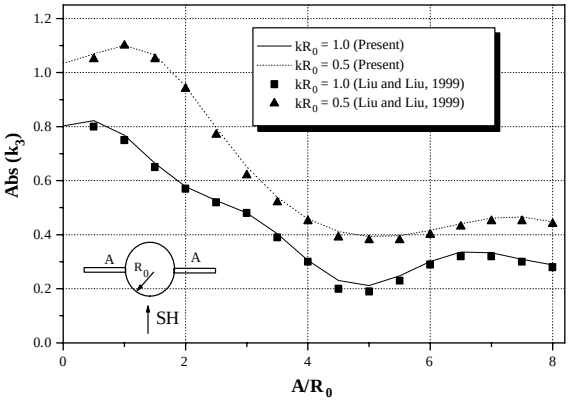

Fig. 4. Results of this paper for the case of two co-linear radial cracks compared with those of Liu and Liu (1999).

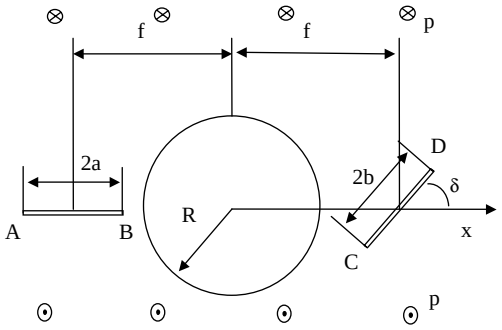

Fig. 5. An infinite region with one circular hole and two cracks subject to static antiplane load.

Table 1
Comparison of our results with those of Chen and Wang (1986)

θ (°)	0°	10°	20°	30°	40°	50°	60°	70°	80°	90°
k_{3A}	1.290	1.288	1.282	1.275	1.267	1.260	1.254	1.250	1.247	1.246
k_{3A*}	1.289	1.287	1.287	1.275	1.267	1.260	1.254	1.250	1.247	1.246
k_{3B}	1.725	1.722	1.712	1.699	1.685	1.672	1.662	1.654	1.649	1.648
k_{3B*}	1.725	1.721	1.712	1.699	1.687	1.672	1.662	1.654	1.649	1.648
k_{3C}	1.725	1.650	1.464	1.233	0.998	0.768	0.547	0.330	0.117	−0.091
k_{3C*}	1.725	1.650	1.463	1.233	0.998	0.768	0.546	0.330	0.117	−0.091
k_{3D}	1.289	1.267	1.204	1.107	0.982	0.835	0.669	0.487	0.294	0.091
k_{3D*}	1.289	1.267	1.204	1.107	0.982	0.835	0.669	0.487	0.294	0.091

Note: k_{3A}, k_{3B}, k_{3C}, k_{3D} are the results of the present paper and k_{3A*}, k_{3B*}, k_{3C*}, k_{3D*} are those of Chen and Wang (1986).

$\alpha = \pi/4$, $\beta = -\pi/4$. Thus, the edge crack is parallel to the x-axis. Assume the incident angle of the plane SH wave is 270° and the incident plane SH wave is given by

$$w^{(\mathrm{I})}(z) = A_{\mathrm{I}}\, \mathrm{e}^{\mathrm{i}k[\cos\gamma x + \sin\gamma y]} \tag{35}$$

where A_{I}, k are the displacement amplitude and the wave number and γ is the incident angle. The dynamic stress intensity factor (DSIF) at the tip B of the crack is expressed as follows

$$K_{3B} = \mu A_{\mathrm{I}} k\sqrt{\pi R}\, k_{3B} \tag{36}$$

In general, the DSIFs take complex values, so only the absolute values of the DSIFs are given here. Results showing the variation of $|k_{3B}|$ versus the non-dimensional wave number kR are given in Fig. 6. The kR in Fig. 6 varies from 0 to 4.0. With the increasing of a/R, the maximum values of $|k_{3B}|$ increase correspondingly. Also, the low frequency resonance phenomenon becomes more pronounced when a/R takes larger value.

4.2.3. The influence of the incidence angle of SH waves on the DSIFs of an edge crack

In this example, we will consider the influence of the incidence angle of the SH wave on the dynamic response of a crack terminating at the boundary of the circular hole. Suppose the tip A of the crack terminates at the hole boundary ($\rho_A = R$) and the tip B is embedded in the homogeneous medium. Let $\alpha = 0$, $\beta = \pi/4$ and let the length of the crack be $2a$. The ratio a/R takes 0.1, 0.3, 0.7, 1.0. The incidence angle of the SH wave takes 0°, 45°, 90°, 135° and 180° and the non-dimensional wave number kR varies from 0 to 4.0. The DSIFs are normalized by Eq. (36). Fig. 7 shows the variation of $|k_{3B}|$ versus the non-dimensional

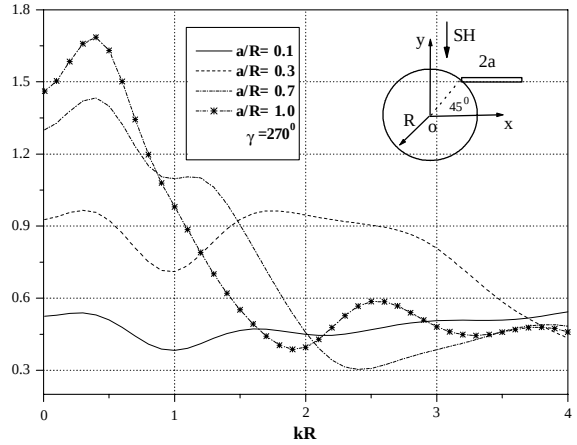

Fig. 6. The influence of the length of an edge crack on its DSIFs with $a/R = 0.1$, 0.3, 0.7, 1.0, incidence angle $\gamma = 270°$ and $kR = 0.0$–4.0.

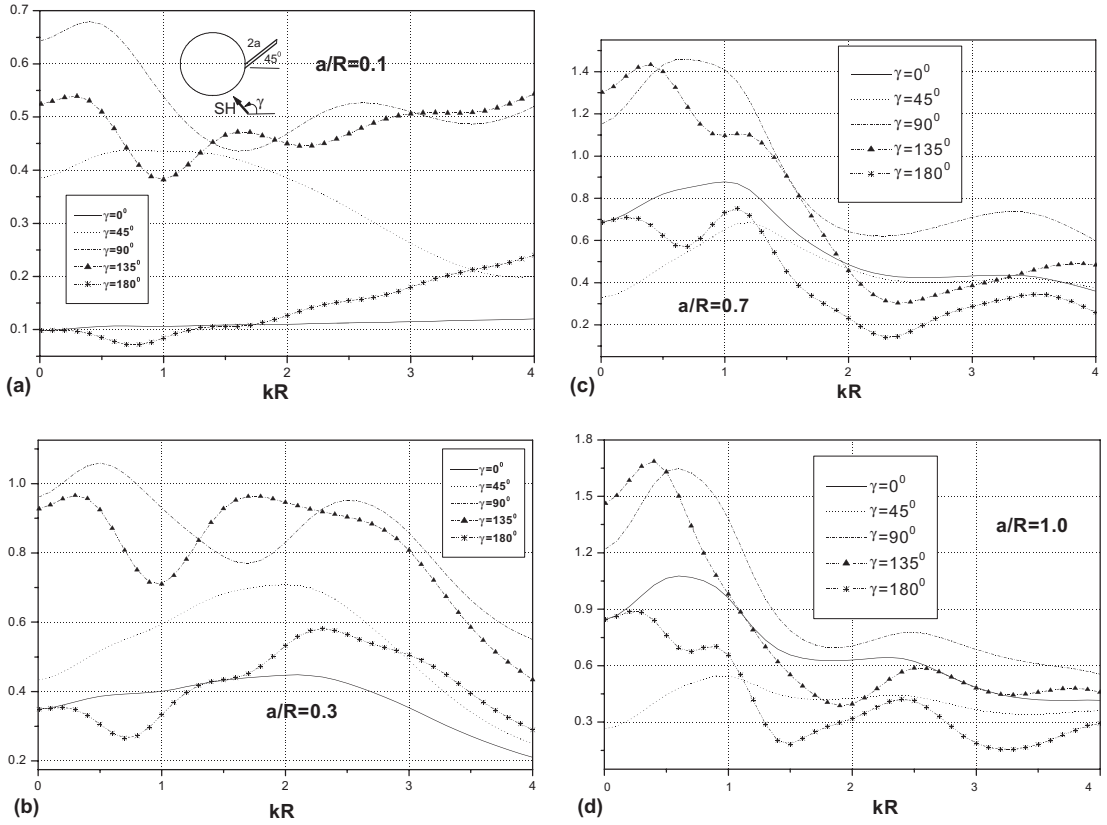

Fig. 7. The influence of the incidence angle of SH waves on the DSIFs of an edge crack with incidence angle $\gamma = 0°$, 45°, 90°, 135°, 180° and $kR = 0.0$–4.0: (a) case for $a/R = 0.1$, (b) case for $a/R = 0.3$, (c) case for $a/R = 0.7$, (d) case for $a/R = 1.0$.

wave number kR for different incident angles. When the incidence angle is 0°, $|k_{3B}|$ takes small value for smaller a/R; but for larger value a/R, $|k_{3B}|$ increases significantly. This is due to the fact that when the incident angle is 0°, the crack is on the shadow side of the hole, so its dynamic response is weak, but when the crack length increases, the crack reaches beyond the shadow region of the hole. Moreover, both the amplitude and the resonance frequency of $|k_{3B}|$ depend on the incident wave significantly. For small values a/R, $|k_{3B}|$ achieves a maximum at 90° incidence angle; but for large value of a/R, $|k_{3B}|$ has a maximum at 135°. In addition, the resonance phenomenon is more obvious for 90° and 135° than for the other incidence angles.

4.2.4. The influence of the obliquity of an edge crack on its DSIFs

In this example, the influence of crack position will be considered. Suppose the tip A of an edge crack terminates at the hole boundary while tip B is embedded in the homogeneous medium. The non-dimensional values of DSIFs are defined in Eq. (36). The calculation parameters are chosen as: $\rho_A = R$, $\alpha = 0$, $-85° \leqslant \beta \leqslant 85°$, $a/R = 0.1$, 0.3, the incident angle of the plane SH wave $\gamma = 90°$ and the non-dimensional wave number $kR = 0.0$, 1.0, 2.0, 3.0, 4.0. Fig. 8 illustrates the variation of $|k_{3B}|$ versus the angle β. For small

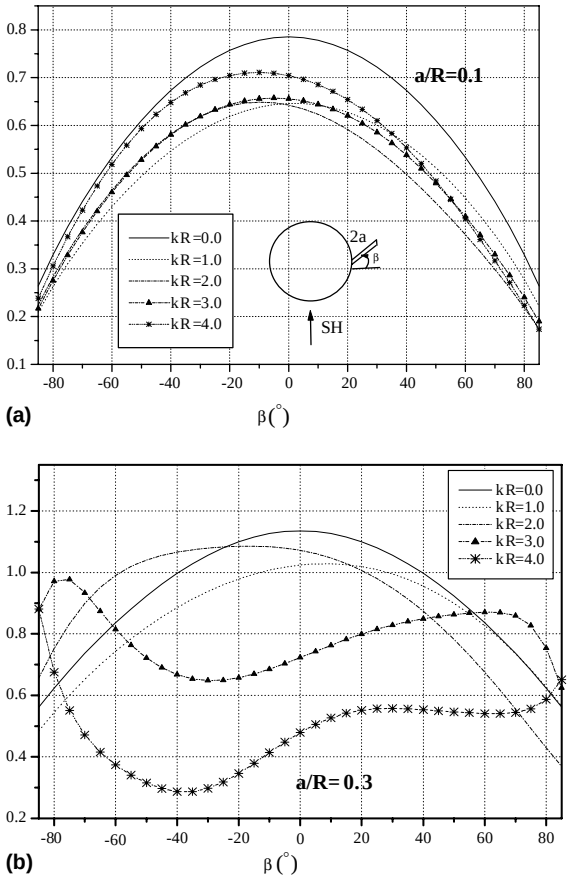

Fig. 8. The influence of the obliquity of an edge crack on its DSIFs with $\beta = -85°$ to 85°, incidence angle $\gamma = 90°$ and $kR = 0.0$, 1.0, 2.0, 3.0, 4.0, respectively: (a) case for $a/R = 0.1$ and (b) case for $a/R = 0.3$.

value kR, $|k_{3B}|$ achieves its maximum when the crack is near the horizontal position, while for larger kR, $|k_{3B}|$ does not achieve maximum at the horizontal position. So for the static and lower frequency problem, the edge cracks normal to the direction of SH wave propagation are more dangerous than others; while for the high frequency case, the dangerous position of the edge cracks depends on the ratio a/R and the wave number of the incident wave.

4.2.5. Two parallel cracks interacting with a circular hole

Consider two cracks L_1, L_2 near the circular hole and the two cracks are parallel to the x-axis. The tips of the two cracks are A_1, B_1 and A_2, B_2 respectively. The lengths of the L_1 and L_2 are $2a_1$ and $2a_2$. Assume the ratio $a_1/R = a_2/R = 0.1$, 0.3, 0.7, 1.0. The midpoints of the two cracks coincide with the y-axis (Fig. 9a). The distances between the cracks and the x-axis are equal to h and $h/R = 1.2$. The incident angle of plane SH wave is 90° (Fig. 9a). The values of DSIFs at the crack tips are normalized by Eq. (36). The variations of $|k_{3A_1}|$, $|k_{3B_1}|$, $|k_{3A_2}|$, $|k_{3B_2}|$ versus the non-dimensional wave number kR for different values of a_1/R, a_2/R are given in Fig. 9. The value kR varies from 0 to 5.0. Fig. 9 shows that for small values of a_1/R and a_2/R, $|k_{3A_1}|$, $|k_{3B_1}|$, $|k_{3A_2}|$, $|k_{3B_2}|$ do not vary significantly with the variation of wave number and the resonance phenomenon is not apparently visible. For larger values of a_1/R, a_2/R, the resonance phenomenon gets more

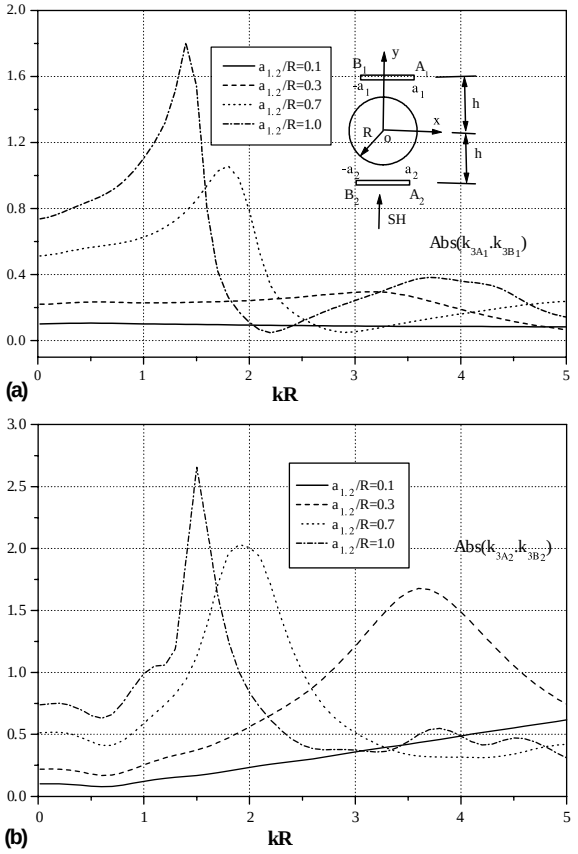

Fig. 9. Two parallel cracks interacting with a circular hole with $kR = 0.0$–5.0, incidence angle $\gamma = 90°$, $h/R = 1.2$ and $a_1/R = a_2/R = 0.1$, 0.3, 0.7, 1.0: (a) results for the tips A_1 and B_1, (b) results for the tips A_2 and B_2.

pronounced: the resonance frequencies decrease; the resonance amplitudes increase considerably; the resonance domains get narrow. It also can be concluded from Fig. 9, that the resonance amplitude of the crack A_2B_2 which is at the incident side of the circular hole are always greater than those of the crack A_1B_1. However, the difference between the resonance amplitudes of the two cracks decreases with increasing crack lengths.

4.2.6. Interaction between an edge crack, an interior crack and a circular hole

In this example the interaction between the two cracks near the circular hole will be considered. Let A_1, B_1 and A_2, B_2 denote the tips of L_1, L_2 respectively. The tip A_2 of the crack L_2 terminates at the hole boundary ($\rho_{A_2} = R$). Suppose $\rho_{A_1} = 1.1R$, $\alpha_1 = 0$, $\beta_1 = 45°$ and $\alpha_2 = 180°$, $\beta_2 = 0°$. Let the lengths of L_1, L_2 be $2a_1$, $2a_2$. The length of L_1 is fixed and $a_1/R = 0.3$, while $a_2/R = 0.1$, 0.3, 0.7, 1.0. The incident angle of the plane SH wave is 90°. The values of DSIFs at tips A_1, B_1, B_2 are normalized by Eq. (36). The variations of $|k_{3A_1}|$, $|k_{3B_1}|$, $|k_{3B_2}|$ for different a_2/R versus non-dimensional wave number kR are given in Fig. 10. With the increasing of a_2/R, $|k_{3B_2}|$ increase significantly. Also, the resonance phenomena of the L_2 are significant when a_2/R increases, while the resonance frequencies vary little. In addition, $|k_{3A_1}|$, $|k_{3B_1}|$ also increase slightly with increasing a_2/R.

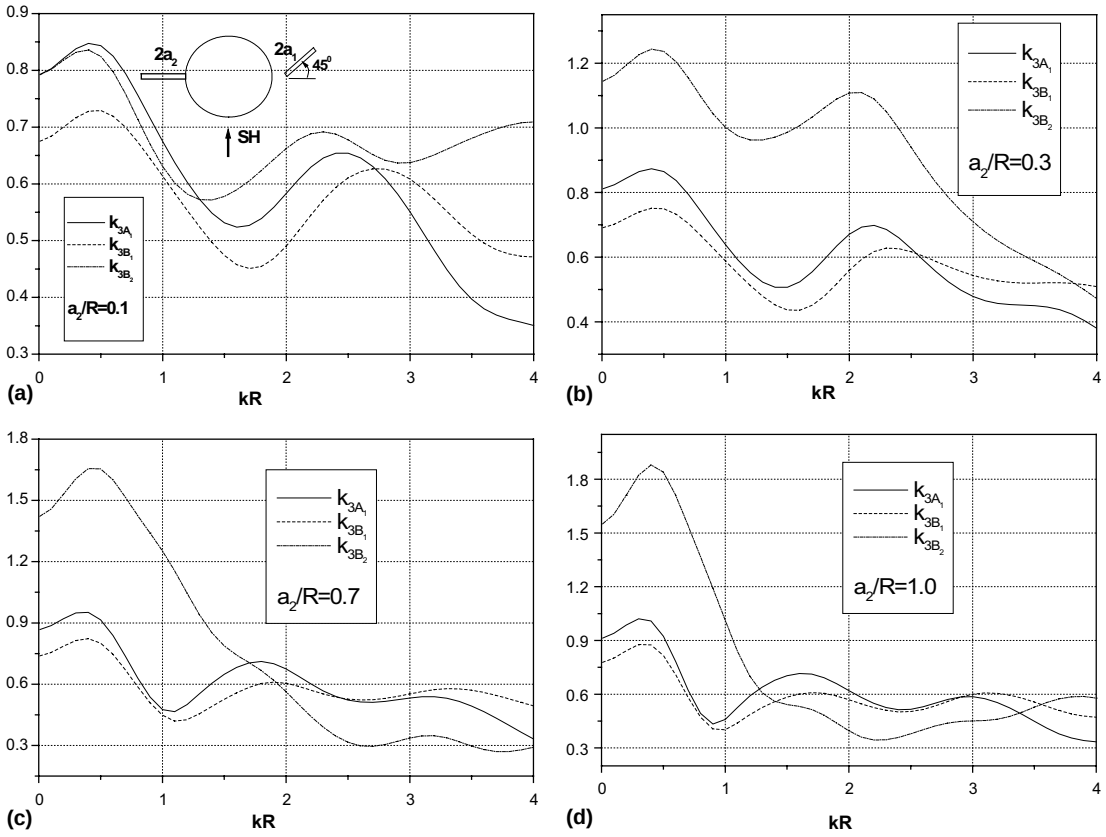

Fig. 10. Interaction between two cracks: an edge crack, an interior crack and a circular hole with $kR = 0.0$–4.0 and incidence angle $\gamma = 90°$: (a) case for $a_2/R = 0.1$, (b) case for $a_2/R = 0.3$, (c) case for $a_2/R = 0.7$, (d) case for $a_2/R = 1.0$.

5. Conclusions

Through above analysis and calculation, we can draw following conclusions:

(1) A special hypersingular integral equation method (HIEM) for solving the dynamic interaction between multiple cracks and a circular hole has been developed in the paper. Our approach is based on the special Green's function for a circular boundary and the resulting hypersingular integral equations. The present method will facilitate the calculation of dynamic crack–hole interaction problem, which is common in practical engineering.
(2) The decomposition method adopted in this paper facilitates the construction of the hypersingular integral equations for multiple cracks. Also, it allows an accurate calculation of the Green's functions even when cracks terminate at the boundary of the circular hole.
(3) Combined with the Fourier transformation method, our method can also be used to analyze transient crack–hole interaction problem. The problem of a crack–hole system subject to concentrated harmonic forces or distributed harmonic forces can also be solved by the proposed method. After the solution of the hypersingular integral equations, the stresses along the boundary of the circular hole can also be calculated by summing the free wave field and the scattered field of the cracks.

Acknowledgements

The research is financed by the Norwegian Scientific Council in the framework of the project 149238/431 "Mathematical formulation of seismic attenuation based on physical models of mechanical rock behavior". The two anonymous reviewers who gave a lot of valuable and pertinent advice concerning the original version of the paper are greatly thanked.

References

Abduljabbar, Z., Datta, S.K., Shah, A.H., 1983. Diffraction of horizontally polarized shear waves by normal edge cracks in a plate. J. Appl. Phys. 54, 461–472.

Abramowitz, M., Stegun, I.A., 1965. Handbook of Mathematical Function. Dover, New York.

Achenbach, J.D., 1973. Wave Propagation in Elastic Solids. North-Holland, Amsterdam.

Boström, A., 2003. Review of hypersingular integral equation method for crack scattering and application to modeling of ultrasonic nondestructive evaluation. Appl. Mech. Rev. 56, 383–405.

Chen, Y.Z., Wang, Z.X., 1986. Solutions of multiple crack problems of a circular region with free or fixed boundary condition in antiplane elasticity. Int. J. Fract. 30, 287–293.

Chen, Y.Z., 1995. Hypersingular integral-equation approach for the multiple crack problem in an infinite-plate. Acta Mech. 108, 121–131.

Crouch, L.S., Starfield, A.M., 1983. Boundary Element Methods in Solid Mechanics. George Allen & Unwin, London.

Cruse, T.A., 1988. Boundary Element Analysis in Computational Fracture Mechanics. Kluwer, Dordrecht.

Cruse, T.A., 1996. BIE fracture mechanics analysis: 25 years of developments. Comput. Mech. 18, 1–11.

Datta, S.K., Shah, A.H., Fortunko, C.M., 1982. Diffraction of medium and long wavelength horizontally polarized shear waves by edge cracks. J. Appl. Phys. 53, 2895–2903.

Gong, S.X., Meguid, S.A., 1991. General solution to the antiplane problem of an arbitrarily located elliptic hole near the tip of a main crack. Int. J. Solids Struct. 28, 249–263.

Gross, D., Zhang, C., 1988. Diffraction of SH waves by a system of cracks: solution by an integral equation method. Int. J. Solids Struct. 24 (1), 41–49.

Hadamard, J., 1923. Lectures on Cauchy's Problem in Linear Partial Equations. Yale University Press.

Ioakimidis, N.I., 1983. A new singular integral equation for the classical crack problem in plane and antiplane elasticity. Int. J. Fract. 21, 115–122.

Kaya, A.C., Erdogan, F., 1987. On the solution of integral equations with a generalized Cauchy kernel. Q. Appl. Math. 15, 455–469.

Krenk, S., Schmidt, H., 1982. Elastic wave scattering by a circular crack. Philos. Trans. R. Soc. London Ser. A 308, 167–198.

Kupradze, V.D., 1965. In: Sneddon, I.N., Hill, R. (Eds.), Progress in Solid Mechanics, vol. III. North-Holland, Amsterdam.
Lachat, J.C., Watson, J.O., 1976. Effective numerical treatment of boundary integral equations: a formulation for three dimensional elastostatics. Int. J. Numer. Meth. Eng. 10, 991–1005.
Lee, V.W., Trifunac, M.D., 1979. Response of tunnels to incident SH waves. J. Engng. Mech. ASCE 105, 643–659.
Liaw, B.M., Kamel, M., 1991. A crack approaching a curvilinear hole in an anisotropic plane under general loadings. Eng. Fract. Mech. 40, 25–35.
Liu, D.K., Liu, H.W., 1999. The scattering of SH wave by edge cracks of a circular hole and the dynamic stress intensity factors. Acta Mech. Sin. 31, 292–299 (Chinese edition).
Liu, S.W., Sung, J.C., Chang, C.S., 1997. Transient scattering of SH waves by surface-breaking and sub-surface cracks. Int. J. Solids Struct. 34, 4019–4035.
Loeber, J.F., Sih, G.C., 1968. Diffraction of antiplane shear waves by a finite crack. J. Acoust. Soc. Am. 44, 90–98.
Lu, J.F., 2000. The interaction between piles and saturated soil. Doctoral Dissertation of Shanghai Jiaotong University, Shanghai, PR China.
Murai, Y., Kawahara, J., Yamashita, T., 1995. Multiple-scattering of SH-waves in 2-D elastic media with distributed cracks. Geophys. J. Int. 122, 925–937.
Muskhelishvili, N.I., 1953a. Singular Integral Equations. Noordhoff, Groningen, Netherlands.
Muskhelishvili, N.I., 1953b. Some Basic Problem of Mathematical Theory of Elasticity. Noordhoff, Groningen, Netherlands.
Neerhoff, F.L., 1979. Diffraction of Love waves by a stress-free crack of finite width in the plane interface of a layered composite. Appl. Sci. Res. 35, 265–315.
Nied, H.F., 1987. Periodic array of cracks in a half-space subjected to arbitrary loading. J. Appl. Mech. ASME 54, 642–646.
Pao, Y.H., Mow, C.C., 1973. Diffraction of Elastic Wave and Dynamic Stress Concentrations. Grane and Russak, New York.
Portela, A., Aliabadi, M.H., 1992. The dual boundary element method: effective implementation for crack problems. Int. J. Numer. Meth. Eng. 33, 1269–1287.
Providakis, C.P., Sotiropoulos, D.A., Beskos, D.E., 1993. BEM analysis of reduced dynamic stress-concentration by multiple holes. Commun. Numer. Methods Eng. 9, 917–924.
Qu, J., 1995. Scattering of plane waves from an interface crack. Int. J. Eng. Sci. 33, 179–194.
Savin, G.N., 1961. Stress Concentration Around Holes. Pergamon Press, New York.
Selcuk, S., Hurd, D.S., Crouch, S.L., Gerberich, W.W., 1994. Prediction of interfacial crack path: a direct boundary integral approach and experimental study. Int. J. Fract. 67, 1–20.
Stone, S.F., Ghosh, M.L., Mal, A.K., 1980. Diffraction of antiplane shear waves by an edge crack. J. Appl. Mech. ASME 47, 359–362.
van den Berg, P.M., 1981. Transition matrix in acoustic scattering by a strip. J. Acoust. Soc. Am. 70, 615–619.
Watson, G.N., 1962. A Treatise on the Theory of Bessel Function. University Press, Cambridge.
Zhang, C., 1991. Dynamic stress intensity factors for periodically spaced collinear antiplane shear cracks between dissimilar media. Theor. Appl. Fract. Mech. 15, 219–227.